JOC The Journal of Organic Chemistry

ARTICLE

pubs.acs.org/joc

On the Memory of Chirality in Gold(I)-Catalyzed Intramolecular Carboalkoxylation of Alkynes

Olalla Nieto Faza,*[,†] Carlos Silva López,[‡] and Angel R. de Lera[‡,*]

[†]Departamento de Química Orgánica, Facultade de Ciencias, Universidade de Vigo, Campus As Lagoas 32004, Ourense, Spain

[‡]Departamento de Química Orgánica, Facultade de Química, Universidade de Vigo, As Lagoas/Marcosende 36310, Vigo, Spain

Supporting Information

ABSTRACT: A computational study of the mechanism of the intramolecular carboalkoxylation of alkynes reported by Toste et al. allows the characterization of the chirality transfer process that makes this reaction enantioselective. Memory of chirality is preserved up until the stereocenter-generating iso-Nazarov cyclization through the synergy between the helicity of a pentadienyl cation intermediate and the control in the conformation of the allyl group, both elements defined upon alkoxy migration. The high barriers to conformational scrambling relative to those corresponding to chemical steps ensure the robustness of the chirality transfer mechanism and result in an unusual importance of conformational changes in reactivity that seems to be common in gold-catalyzed transformations.

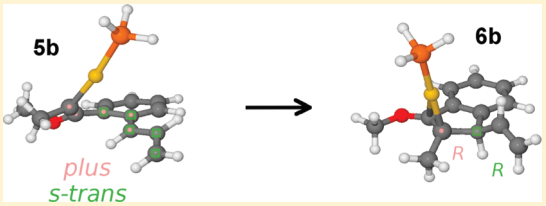

The use of gold(I) and gold(III) homogeneous catalysis has seen an exciting development in recent years.[1] The use of gold salts and complexes in catalysis leads to the formation of carbon−carbon and carbon−heteroatom bonds in transformations that combine mild reaction conditions and compatibility with a wide selection of functional groups with impressive increase in molecular complexity and structural diversity. Most examples of such processes described in the literature involve gold acting as a soft carbophilic Lewis acid which activates alkynes, allenes, or alkenes toward nucleophilic attack.[1,2] The rich reactivity that follows this activation depends on the structure of the substrate, and sometimes it involves a cascade of steps where further intervention of gold is needed. A good example of this kind of gold catalysis is found in enyne cycloisomerizations[3,1d] or the reactions of propargyl esters,[4] two well studied manifolds where three main reactivity paradigms are available for further evolution: direct nucleophilic attack to the activated unsaturation, domino reactions with formation of allene intermediates, or processes induced by carbenoid gold formation.

Despite their avidity for unsaturated C−C bonds, gold complexes have a non-negligible affinity toward heteroatoms that has been the object of recent interesting developments.[5] This dual character can lead to reactivity patterns where sequential gold π-coordination to unsaturations and σ-coordination to heteroatoms are involved in more complex transformations.[6]

Despite the starting point in homogeneous gold catalysis being the first asymmetric aldol reaction,[7] in view of the surge of results describing new reactions through homogeneous gold catalysis and the use of gold salts to achieve known transformations more efficiently, the development of stereoselective versions seems to be lagging behind. However, these reactions oftentimes proceed with very good selectivities, resulting in complex structures of controlled stereochemistry, a fact that has been receiving increasing attention, with numerous examples of stereoselective gold-catalyzed reactions reported in the literature.[8]

Diastereo- and enantioselective homogeneous gold-catalyzed reactions can be achieved through three different strategies: (i) chiral ligands on the metallic center as in the enantioselective hydroalkoxylation of allenes[9] or hydrogenation of alkenes;[10] (ii) chiral counterions, through ion-pair formation in the hydroalkoxylation of allenes;[11] (iii) transfer of chiral information from the substrate to products.

For a long time, it was thought that the use of chiral ligands on gold complexes would not be effective, due to the linear geometry at the metal center, which places the stereogenic elements far from the reaction site, but some chiral phosphine ligands have provided encouraging results.[9,10] Toste et al. have developed the concept of using a chiral counterion, not directly attached to the metal, to achieve stereocontrol in gold catalysis,[11] but the scope of the method has not been completely explored yet. Thus, the transfer of chiral information between a stereogenic center or axis in the substrate and a center in the product remains a widely reported strategy for performing stereoselective gold-catalyzed reactions. Allenes are common chiral groups involved in chirality transfer, as exemplified in the transformation of β-hydroxy or amino allenes into dihydropyrans and tetrahydropyridines[12] or of α-hydroxy allenes into dihydrofurans.[13] However, many examples are being developed where the configuration of an alcohol, ester, or ether function, or even an epoxide, determines the configuration of a new center created in the reaction, such as the enantioselective propargyl Claisen

Received: January 13, 2011
Published: March 28, 2011

rearrangement,[14] the tandem Claisen rearrangement/heterocyclization used in the synthesis of dihydropyrans,[15] the synthesis of spiropyranones from epoxyalkynes[16] or the Rautenstrauch reaction.[17]

Recently, Toste et al. described an intramolecular carboalkoxylation of alkynyl ethers (**I**) where chirality is transferred from the stereogenic benzyl center to the new stereogenic center generated in the methoxy indene product **II** via the cyclization of a helical gold allyl benzyl cation (see Figure 1).[18] The similarities between the proposed mechanism and the results of our previous work on the center-to-helix-to-center chirality transfer found in the gold-catalyzed Rautenstrauch reaction[19] prompted us to address in detail how the chiral information is preserved and transformed along the reaction path.

For this, we located the stationary points along the reaction coordinate for the system depicted in Figure 2. This system is one of those used in the experiments, for which a good yield (92%) and enantiomeric excess of 95% was found. The only modification introduced, for the sake of reducing the computational cost, is the replacement of a phenyl group at the terminal alkyne with a methyl residue, and the use of PH_3 as a model of the triphenylphosphine used in the experimental work. This truncation of the ligand has produced good results in systems where gold's role is just to provide π-acid activation through linear complexes that place gold's ligand far from the reactive center.[20]

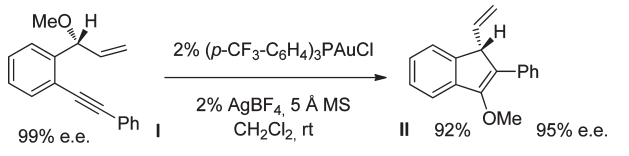

Figure 1. Stereoselective gold(I)-catalyzed intramolecular carboalkoxylation of alkynes described by Toste et al.[18]

In Figure 2 the stationary points in the transformation of **1** into **7** (corresponding to the mirror images of **I** and **II** in Figure 1, respectively) are depicted. The alkyne−gold complex **2** is considered the starting point of the catalytic cycle, and the origin of energies. In the gas phase, the preferred conformation of **2** places gold *syn* to the methoxy group due to electrostatic effects (4.17 kcal/mol more stable than the *anti* complex). The alternative structure, where **1** coordinates to gold through the ether oxygen (**2b**), lies 2.53 kcal/mol below **2**. This latter fact could point toward an alternate mechanism, based on ether activation; nevertheless, both the experimental findings of Toste et al.[18] and the high energies for the transition structures involved in the early steps of this path led us to discard this parallel mechanism. The gold-assisted dealkoxylation of **1** (**ts28**) is a highly unfavorable process with a barrier of 32.12 kcal/mol (11 kcal/mol higher than the rate-limiting step in the alkyne activation mechanism), and the next transition state, corresponding to the concerted nucleophilic attacks of the gold-coordinated alkoxide to the alkyne and of the alkyne to the resultant resonance-stabilized cation (**ts87**) that leads to the product, is even higher in energy.[21]

After π-coordination of **1** with gold, the alkoxy oxygen in **2** attacks the activated alkyne to yield the cationic gold−alkylideneisobenzofuran intermediate **3**. The relative orientation of the nucleophile and the metal in this transition structure is anti, as expected from steric arguments.[22] Even if two paths can be proposed for this step, only one transition structure (**ts23a**) was found. The fact that every attempt to locate the alternative **ts23b** converged to **ts23a** is not unexpected, since the only difference between the products of this step (**3a** and **3b**) is conformational: the puckering of the alkylidene isobenzofuran ring.

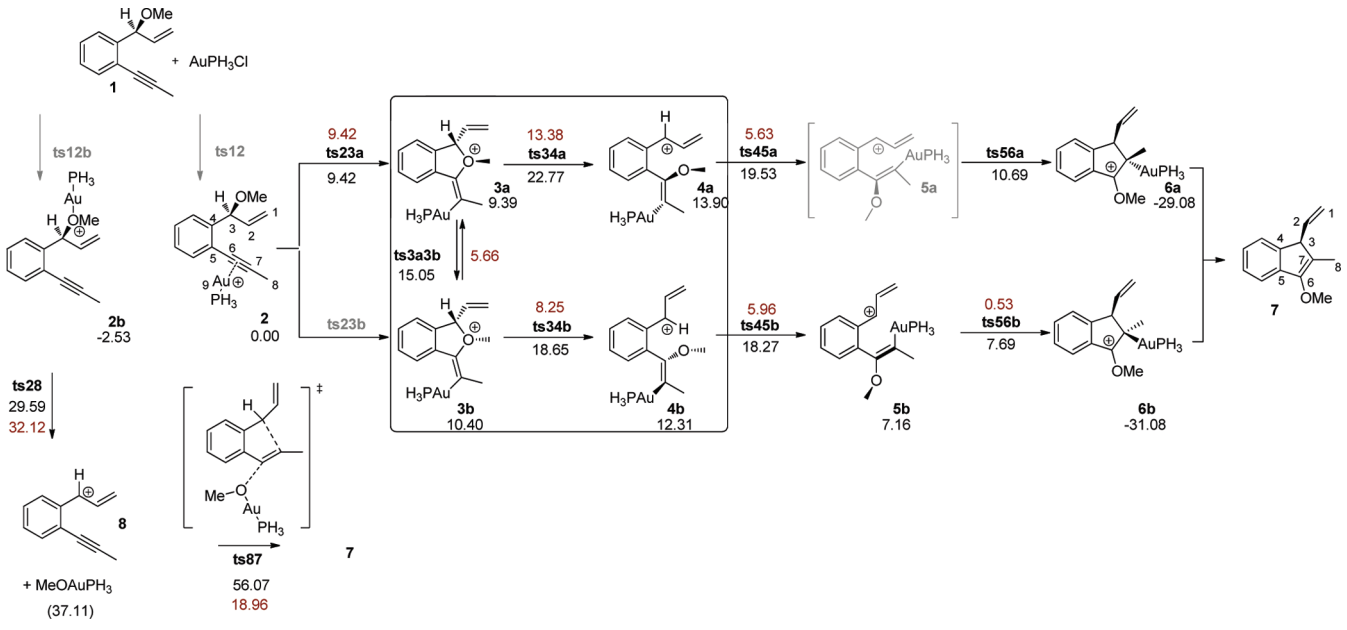

Figure 2. Available reaction paths for the gold(I)-catalyzed intramolecular carboalkoxylation of alkyne **1**. With the alkyne−gold complex **2** as the origin of energies, Gibbs free energies (in kcal/mol) of all the stationary points are shown in black and activation barriers shown in red below and above the corresponding arrows, respectively. Two paths are shown after **2**, depending on the orientation of the alkyne undergoing gold-catalyzed carbon−heteroatom bond formation and the resultant conformation of the cationic alkylidene isobenzofuran intermediate **3**. The key step in determining the selectivity, the C_3−O bond cleavage (**ts34**) leading to a pentadienyl backbone with helical chirality (**4**), is highlighted inside a square box. An alternative path corresponding to a noncompetitive ether activation (on the left) is also shown for reference.

dx.doi.org/10.1021/jo200090j |*J. Org. Chem.* 2011, 76, 3791–3796

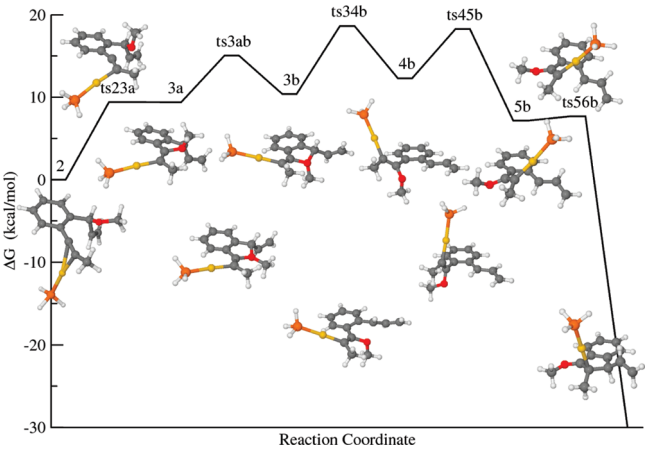

Figure 3. Schematic free energy profile for the transformation of **2** into **6**.

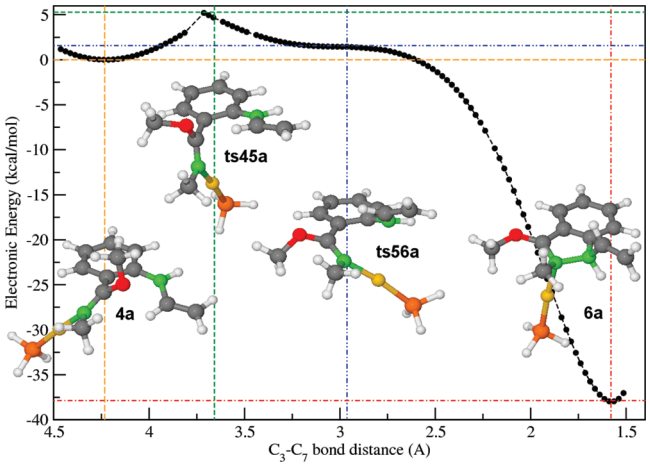

Figure 4. B3LYP/6-31G*-SDD electronic energy (in kcal/mol) vs C_3-C_7 distance in the region between **4a** and **6a**. The points along this one-dimensional potential energy surface have been calculated using constrained optimizations with frozen C_3-C_7 distance. The intersection of straight lines on the graph signals the location in terms of electronic energy and C_3-C_7 distance, of the fully optimized stationary points. Their geometries overlap well with those of the corresponding points in the scan, and only for **ts45a** is there a slight variation in the C_3-C_7 distance, albeit not in the energy. C_3 and C_7 are shown in green for convenience.

As can be seen in Figure 2, the reactive conformation of **3** will determine the further evolution of the system, differentiating between two branches (*a* and *b*) in the mechanism. The *a* branch is characterized by the *in* disposition of the vinyl group in the allyl cation, while the *out* conformation is adopted by the structures along *b*. If there were no interconversion between them, **3a** would evolve through the upper branch while **3b** would follow the lower path in Figure 2. Since **3a** is the direct product of the nucleophilic attack (**ts23a**), and more stable than **3b** by 1 kcal/mol, the *a* branch would be the expected reaction path (see Figure 3). Nevertheless, the barrier for the interconversion of the two conformers (**ts3a3b**) and for the C_3-O bond cleavage on **3b** (**ts34b**) are 4.12 kcal/mol lower than the barrier for the corresponding bond scission in **3a** (**ts34a**), signaling the *b* branch in Figure 2 as the preferred path. The energy values found along this path, consistently lower than the energies of the corresponding structures with the *in* vinyl group, due to steric effects, also confirm this conclusion. We find interesting, however, to continue the description of both the *a* and *b* branches in parallel, even if *a* is noncompetitive.

The next step involves the cleavage of the C_3-O bond to yield pentadienyl cations **4a** and **4b**. The structure of the transition states involved, and consequently the geometry of **4**, is a direct consequence of the conformation of **3**: the bond rotations upon the opening of **3a** leave an *in* vinyl group and a *plus* helix, while the opening of **3b** leads to the *minus* helix and *out* vinyl group. As explained below, the combination of these two elements is key in ensuring the transfer of the chiral information from **1** to **7**. Despite its low barrier (8.25 kcal/mol), which is due to the relatively high energy of **3**, this is also the rate-limiting step in the mechanism.

The main geometrical changes[23] upon the alkoxy migration from **2** to **4** are the result of the transfer of the formal positive charge from the metal center to C_3. With the formation of this new unsaturated center, now we have a fully conjugated chain that can be seen as a pentadienyl cation. Even if the bond lengths in the carbon skeleton of the molecule reflect the effects of this enhanced conjugation, the largest variation is found for the C_3-C_4 bond, whose shortening by around 0.12 Å with respect to **2** (compared to the 0.09 Å found for the C_2-C_3 bond) denotes a carbocation preferentially delocalized over the aromatic ring. Another salient feature is the consolidation of the elongation of the C_6-C_7 bond, already present in **3**, upon completion of the alkoxylation of the activated alkyne in **2** (this distance is 1.25, 1.33, and 1.37 Å in **2**, **3**, and **4**, respectively). This change from η^2-coordination to an alkyne to σ-bonding to an alkene is also reflected in the $Au-C_7$ distances (and the corresponding bond angles), that are 0.10 and 0.11 Å shorter in **3** and **4** than in **2**.

After **4**, clockwise rotation (about 110°) of the C_5-C_6 bond leaves the σ-gold-coordinated alkene in the appropriate conformation for subsequent nucleophilic attack to the allyl-benzyl cation and results in a formal inversion of the helix (now the methoxy group is replaced by the vinyl gold as part of the helix, and **5b** sports a *plus* helicity) and gold in an *in* position. Steric crowding prevents rotation in the opposite direction, which would involve transition states where a methoxy group is in the same plane as the vinyl substituent. The transition structures corresponding to this conformational change do not involve any interaction with the vinyl moiety, so their energies are similar in the two branches of the mechanism. However, that is not the case of intermediates **5**. While pentadienyl cation **5b** is a well-defined minimum with an energy (7.16 kcal/mol) comparable to that of the previous intermediates, a stationary point corresponding to **5a** could not be located on the potential energy surface between the well characterized transition states **ts45a** and **ts56a**. The steric interaction between the bulky gold fragment and the *in* vinyl group so greatly distorts the near planarity of this pentadienyl cation that the minimum gets confused with the ring-closing transition structure. This can be inferred from a series of constrained geometry optimizations that span values of the C_3-C_7 distance between those found in **4a** and **6a**, and from the resultant plot of electronic energy vs C_3-C_7 distance shown in Figure 4.[24]

The graph in Figure 4 indicates the difficulties in locating the minimum **5a** on a potential energy surface that is extremely planar and seems to connect **4a** and **6a** through a single transition state **ts45a** followed by a barrierless cyclization. Thus, the characterization of structure **ts56a** as either a shallow minimun or a transition state can be proposed, especially when the imaginary frequency associated to the C_3-C_7 stretching and the rotation of the two sp^2 centers is very low (-8.38 cm^{-1}).

dx.doi.org/10.1021/jo200090j |*J. Org. Chem.* 2011, 76, 3791–3796

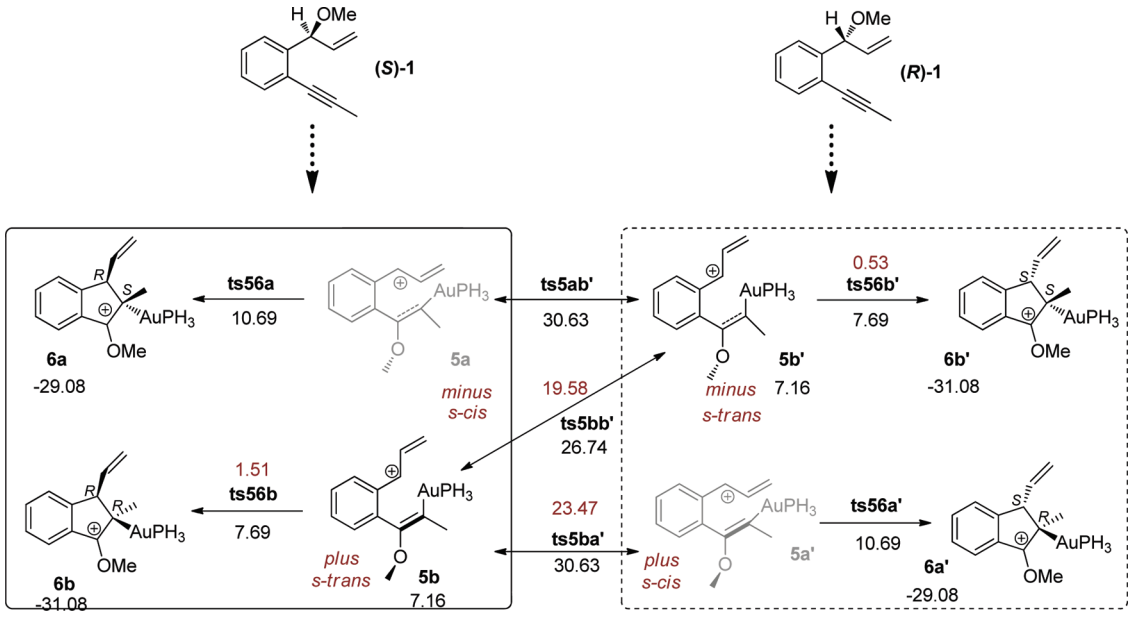

Figure 5. Representation of the hypothetical mechanisms that could produce conformational scrambling along the **2** → **7** reaction path, leading to the enantiomer of **7**. Gibbs free energies (in kcal/mol relative to **2**) of all the stationary points are shown in black, and activation barriers are shown in red near the corresponding arrows. Enantiomers of the structures depicted in Figure 2 are denoted with apostrophes.

Once the helical pentadienyl conformation of the gold cation has been reached (**5**), a C−C bond-forming process ensues that could be defined as either a conrotatory four-electron electrocyclization or the nucleophilic attack of an electron-rich alkene to an allylbenzyl cation. This reaction displays features similar to that of the iso-Nazarov cyclization in hydroxyheptatrienyl cations, and, as in these systems, torquoselectivity (preference for **ts56b** over **ts56a**) results from the destabilizing effect of an *inward* vinyl substituent on one terminus of the cyclizing pentadienyl cation.[25]

As is common in this kind of charged and/or very polarized conjugated system, the frontier between pericyclic and ionic processes is unclear.[26,27] Calculation of the NICS[28] along an axis perpendicular to the ring plane suggests certain aromatic character for this transition structure (the profile has a maximum on each side of the plane, very near the center, that would correspond to the maximum density region of the p orbitals involved in the process), but the maximum value is considerably lower (∼6 compared to ∼8 ppm) than that obtained for the analogous transition state in the gold-catalyzed Rautenstrauch reaction[19] and much lower than the NICS values found for purely pericyclic processes (∼11 ppm).[28] This can be explained through both the polarization induced by the methoxy group and by the Au−C bond and through the reluctance of the benzene ring to compromise its aromaticity if too involved in the charge delocalization over the pentadienyl system. Analysis of the anisotropy of the induced charge density (ACID[29]) also points toward a borderline mechanism, with the presence of a small ring current (with a low critical isosurface value of 0.030).

The extremely low value found for the energy barrier of the cyclization (0.53 kcal/mol for **ts56b**, a nearly barrierless process along the *a* branch) can also be rationalized using our previous results on the effect of a donor substituent on C_6 (OMe)[30] and an alkene gold on Nazarov-like reactions.[26,27]

Following a cascade of low-barrier steps (between ∼0.5−9 kcal/mol) that connect intermediates lying within a narrow window of energies (∼5 kcal/mol) that makes them potentially reversible, this last step leads to a very stable structure **6** that is unlikely to revert. Elimination of gold from **6** yields finally a single enantiomer of the reaction product **7**.

Following the two branches of the mechanism in Figure 2, we have shown that the chiral information in **1** is faithfully transferred to the product **7**. This system of chirality transfer is robust and relies in the interplay between both the helicity of the pentadienyl cation intermediate and the *s-cis* or *s-trans* conformation of the allyl substituent. The *plus* helix in **5b**, which is a result of the *minus* helix in **4b**, which stems on its turn from the puckering of the alkylidene-isobenzofuran ring in **3b** determines the rotation taking place at the cyclizing termini and the *R* configuration of C_7 in **6b** as a result. For a given rotation (that is, for a given helix), the configuration of C_3 will depend on the conformation of the vinyl group, with *s-trans* and a *plus* helix leading to *R* configuration at C_3, as found in **6b** for example. Thus, the fact that the opening of **3a** yields *plus-s-cis*-**4a** that evolves to the *minus-s-cis*-**5a**, while **3b** results in the opposite configuration of both elements, guarantees that no matter which of the two paths is followed, the (*R*)-**7** product will be obtained from (*S*)-**1** (upon elimination of gold, the chirality of the second stereogenic center generated in the cyclization is lost).

However, the role of the helicity of the pentadienyl intermediate and the conformation of the allyl cation in the configuration of the product is better understood by referring to Figure 5. In this figure, the carbocyclization step of the two paths (*a* and *b*) available from (*S*)-**1** are highlighted inside a square box, while the pentadienyl cations obtained from the enantiomeric reactant ((*R*)-**1**) through the corresponding enantiomorphic paths are shown to lead to an (*S*) configuration of C_3 in the product. In this manifold, *s-trans* (*s-cis*) conformation of the vinyl group in **5** places gold and vinyl on the same side (opposite sides) of the product **6**, and the *plus* (*minus*) helix leads to an *R* (*S*) configuration at C_7.

When considering this scheme, however, the question arises whether the elements in the helix-allyl conformation combinations obtained from the controlled ring-opening in **ts34** can be

dx.doi.org/10.1021/jo200090j |*J. Org. Chem.* 2011, 76, 3791–3796

modified independently. The result of such scrambling would be either inversion in the configuration of the product or a decrease in the enantiomeric excess (eventually, even obtention of **7** as a racemate). Within this framework, we explored the possibility of the two kinds of conformational changes required for this decoupling of the two elements: either a rotation of the $C_2-C_3-C_4-C_5$ dihedral (switch from *s-cis* to *s-trans*) or an inversion of the pentadienyl cation helicity through a planar transition state on **4** or **5**. We localized a model transition structure for the former in **ts5ab′** and for the latter in **ts5bb′**. The high activation energies of these two processes (that can be extrapolated to the analogous transformations on **4a** or **4b**), 23.47 and 19.58 kcal/mol, respectively, ensure that the flow of chiral information from **1** to **7** depicted in Figure 2 is not disrupted.

In this work, we have computationally characterized the mechanism of the intramolecular carboalkoxylation of alkynes reported by Toste et al.[18] and described in detail the memory of chirality[31] that makes this process enantioselective. In line with our previous findings on the center-to-helix-to-center chirality transfer in the gold-catalyzed Rautenstrauch reaction, we conclude that the helicity of a pentadienyl cation intermediate, a scaffold usually considered planar, is a key element in the information flow. However, for it to be effective, control in the conformation of the allyl group is also needed. The synergy between these two elements, which become defined on alkoxy migration, preserved by high barriers to conformational scrambling, results in the correct product configuration through any of the two potentially competitive paths *a* and *b* in Figure 2, making the chirality transfer mechanism quite robust.

This mechanism is also a good example of a commonly found phenomenon in gold-catalyzed transformations: the low barriers found for the chemical steps in these reactions, denoting mild reaction conditions, result in an uncommon importance of the barriers corresponding to conformational changes (single bond rotations, helix inversions, etc.) on the intermediates, which suddenly can become rate-limiting steps, thus preventing the conformational scrambling that would be expected at these points in more conventional mechanisms.

COMPUTATIONAL DETAILS

The calculations have been performed using the Gaussian 03[32] and Orca[33] packages. Density functional theory in the Kohn−Sham formulation[34] has been used with the Becke three-parameter exchange functional and the nonlocal correlation functional of Lee, Yang, and Parr (B3LYP) to obtain optimized geometries in Gaussian 03.[35] The 6-31G* basis set was used for all atoms except for gold, for which the Stuttgart−Dresden effective core potential[36] and the corresponding basis set were used to accurately take relativistic effects into account and substantially reduce the number of electrons in the system and the computational costs. The wave functions of the optimized structures were shown to correspond to minima in the configuration space.[37]

The stationary points thus obtained were characterized by means of harmonic analysis, and for all the transition structures, the normal mode related to the imaginary frequency corresponds to the nuclear motion along the reaction coordinate under study. In several significant cases, intrinsic reaction coordinate (IRC)[38] calculations were performed to unambiguously connect transition structures with reactants and products. In the transformation between **4a** and **6a**, no stable intermediate could be found corresponding to the structure of **5a**, so a set of constrainted optimizations scanning the C_3-C_7 distance were performed to describe the potential energy surface in this region.

Higher level single point calculations were performed with Orca at the B3LYP optimized geometries in order to provide improved energy values.[39] This energy refinement was carried out with Grimme's double hybrid functional B2PLYP[40] using the RI approximation for coulomb and exchange (RI-JK). The TZVPP[41] basis set has been used for all main group elements and the def2-TZVPP[42] basis with the sd(60,mdf) electron core potential[43] for gold, with the corresponding auxiliary basis.[44] Thermal corrections to the free energy were taken from the previous low-level frequency calculations.[45]

Calculation of the nuclear independent chemical shifts (NICS) have been performed on **ts56b** at the B3LYP/6-31G*-SDD level at points distributed along an axis perpendicular to the ring center and crossing it. The maximum value (6.4 ppm) is found 0.4 Å away from the ring plane (see Figure S1 in the Supporting Information). A calculation of the anisotropy of the induced charge density (ACID)[29] has also been performed for this structure at the same level, a representation of the isosurface corresponding to the critical isosurface value (0.030) can be found in the Supporting Information (Figure S2).

ASSOCIATED CONTENT

Supporting Information. A representation of the NICS and ACID results reported in the text, and Cartesian coordinates of all the stationary points described and the structures in the IRC, together with tables of the corresponding geometric and thermodynamic parameters. This material is available free of charge via the Internet at http://pubs.acs.org.

AUTHOR INFORMATION

Corresponding Author

*E-mail: faza@uvigo.es; qolera@uvigo.es.

ACKNOWLEDGMENT

We thank CESGA for the allocation of computer time. C.S.L. thanks the Xunta de Galicia for his Parga Pondal contract.

REFERENCES

(1) (a) Shapiro, N. D.; Toste, F. D. *Synlett* **2010**, 675–691. (b) Wang, S.; Zhang, G.; Zhang, L. *Synlett* **2010**, 692–706. (c) Michelet, V.; Toullec, P. Y.; Genet, J. P. *Angew. Chem., Int. Ed.* **2008**, *47*, 4268–4315. (d) Jiménez-Núñez, E.; Echavarren, A. M. *Chem. Rev.* **2008**, *108*, 3326–3350. (e) Gorin, D. J.; Toste, D. *Nature* **2007**, *446*, 395–403. (f) Hashmi, A. S. K. *Chem. Rev.* **2007**, *107*, 3180–3211. (g) Fürstner, A.; Davies, P. W. *Angew. Chem., Int. Ed.* **2007**, *46*, 3410–3449.

(2) Widenhoefer, R. A.; Han, X. *Eur. J. Org. Chem.* **2006**, *20*, 4555–4563.

(3) (a) Ma, S.; Yu, S.; Gu, Z. *Angew. Chem., Int. Ed.* **2006**, *45*, 200–203. (b) Soriano, E.; Marco-Contelles, J. *Acc. Chem. Res.* **2009**, *42*, 1026–1036.

(4) Correa, A.; Marion, N.; Fensterbank, L.; Malacria, M.; Nolan, S. P.; Cavallo, L. *Angew. Chem., Int. Ed.* **2008**, *47*, 718–721.

(5) (a) Aponick, A.; Li, C.; Berenger, B. *Org. Lett.* **2008**, *10*, 669–671. (b) Marion, N.; Carlqvist, P.; Gealageas, R.; de Frémont, P.; Maseras, F.; Nolan, S. P. *Chem.—Eur. J.* **2007**, *13*, 6437–6451. (c) Sromek, A. W.; Rubina, M.; Gevorgyan, V. *J. Am. Chem. Soc.* **2005**, *127*, 10500–10501. (d) Nijamudheen, A.; Jose, D.; Datta, A. *J. Phys. Chem. C* **2011**, *115*, 2187–2195.

(6) (a) Cordonnier, M. C.; Blanc, A.; Pale, P. *Org. Lett.* **2008**, *10*, 1569–1572. (b) González-Pérez, A.; Silva, C.; Marco-Contelles, J. L.; Faza, O. N.; Soriano, E.; de Lera, A. R. *J. Org. Chem.* **2009**, *74*, 2982–2991.

(7) Ito, Y.; Sawamura, M.; Hayashi, T. *J. Am. Chem. Soc.* **1996**, *108*, 6405–6406.

(8) Bongers, N.; Krause, N. *Angew. Chem., Int. Ed.* **2008**, *47*, 2178–2181.
(9) (a) Zhang, Z.; Widenhoefer, R. A. *Angew. Chem., Int. Ed.* **2007**, *46*, 283–285. (b) Muñoz, M. P.; Adrio, J.; Carretero, J. C.; Echavarren, A. M. *Organometallics* **2005**, *24*, 1293–1300.
(10) González-Arellano, C.; Corma, A.; Iglesias, M.; Sánchez, F. *Chem. Commun.* **2005**, 3451–3453.
(11) Hamilton, G. L.; Kang, E. J.; Mba, M.; Toste, D. *Science* **2007**, *317*, 496–499.
(12) Gockel, B.; Krause, N. *Org. Lett.* **2006**, *8*, 4485–4488.
(13) Hoffmann-Röder, A.; Krause, N. *Org. Lett.* **2001**, *3*, 2537–2538.
(14) Sherry, B. D.; Toste, F. D. *J. Am. Chem. Soc.* **2004**, *126*, 15978–15979.
(15) Sherry, B. D.; Maus, L.; Laforteza, B. N.; Toste, F. D. *J. Am. Chem. Soc.* **2006**, *128*, 8132–8133.
(16) Shu, X.; Liu, X.; Ji, K.; Xiao, H.; Liang, Y. *Chem.—Eur. J.* **2008**, *14*, 5282–5290.
(17) Shi, X.; Gorin, D. J.; Toste, F. D. *J. Am. Chem. Soc.* **2005**, *127*, 5802–5803.
(18) Dubé, P.; Toste, D. *J. Am. Chem. Soc.* **2006**, *128*, 12062–12063.
(19) Faza, O. N.; Silva, C.; Álvarez, R.; de Lera, A. R. *J. Am. Chem. Soc.* **2006**, *128*, 2434–2437.
(20) Zhang, J.; Shen, W.; Li, L.; Li, M. *Organometallics* **2009**, *28*, 3129–3139. (b) Dudnik, A. S.; Xia, Y.; Li, Y.; Gevorgyan, V. *J. Am. Chem. Soc.* **2010**, *132*, 7645–7655.
(21) Another possible evolution of the system after **8** would be nucleophilic attack of a free alkoxide on a gold-activated alkyne, to yield structures analogous to **4** or **5**. Analysis of all the transition states characterized for such a step seem to point to the previous formation of a C−O bond on the aromatic ring. One of them is only slightly lower in energy than **ts87** (53.51 kcal/mol with respect to **2**, vs 56.07 kcal/mol); the other is significantly more energetic (72.79 kcal/mol), further supporting the inviability of this path.
(22) The analogous *syn* transition structure is 7.41 kcal/mol more energetic than **ts23a**.
(23) See Supporting Information for tables with the most relevant geometric parameters.
(24) The choice of the C_3-C_7 bond distance as a reaction coordinate in this graph poses some problems in the region between **4a** and **ts45a**, since the rotation of the $C_4-C_5-C_6-C_7$ dihedral, the actual reaction coordinate of this first step, is only described through its coupling with the C_3-C_7 elongation. Thus, the overlap of **ts45a** and the structure associated to the maximum in this one-dimensional potential energy surface is not perfect, with a slightly shorter C_3-C_7 distance for the latter, even if their electronic energies are surprisingly close. After **ts45**, though, the chosen reaction coordinate seems to accurately describe the transformations taking place, and the structure and relative energy of **ts56a** closely correspond to a point in the curve.
(25) Faza, O. N.; Silva, C.; Álvarez, R.; de Lera, A. R. *Chem.—Eur. J.* **2009**, *15*, 1944–1956.
(26) Faza, O. N.; Silva, C.; Álvarez, R.; de Lera, A. R. *Chem.—Eur. J.* **2004**, *10*, 4324–4333.
(27) Faza, O. N.; Silva, C.; Álvarez, R.; de Lera, A. R. *Chem. Commun.* **2005**, 4285–4287.
(28) Schleyer, P. v. R.; Maerker, C.; Dransfeld, A.; Jiao, H.; v. Eikema Hommes, N. J. R. *J. Am. Chem. Soc.* **1996**, *118*, 6317–6318.
(29) Geuenich, D.; Hess, K.; Köhler, F.; Herges, R. *Chem. Rev.* **2005**, *105*, 3758–3772.
(30) Along the reaction coordinate of a pentadienyl cation cyclization, there is a displacement of the positive charge from odd to even positions, so a donor on an even position will at the same time stabilize the transition state and the product and destabilize the reactant, resulting in a lower barrier for the reaction. Such a substitution also contributes to a larger polarization of the cycling chain, which also helps lower the activation energy.
(31) Zhao, H.; Hsu, D. C.; Carlier, P. R. *Synthesis* **2005**, 1–16.
(32) Frisch, M. J.; Trucks, G. W.; Schlegel, H. B.; Scuseria, G. E.; Robb, M. A.; Cheeseman, J. R.; Montgomery, J. A., Jr.; Vreven, T.; Kudin, K. N.; Burant, J. C.; Millam, J. M.; Iyengar, S. S.; Tomasi, J.; Barone, V.; Mennucci, B.; Cossi, M.; Scalmani, G.; Rega, N.; Petersson, G. A.; Nakatsuji, H.; Hada, M.; Ehara, M.; Toyota, K.; Fukuda, R.; Hasegawa, J.; Ishida, M.; Nakajima, T.; Honda, Y.; Kitao, O.; Nakai, H.; Klene, M.; Li, X.; Knox, J. E.; Hratchian, H. P.; Cross, J. B.; Bakken, V.; Adamo, C.; Jaramillo, J.; Gomperts, R.; Stratmann, R. E.; Yazyev, O.; Austin, A. J.; Cammi, R.; Pomelli, C.; Ochterski, J. W.; Ayala, P. Y.; Morokuma, K.; Voth, G. A.; Salvador, P.; Dannenberg, J. J.; Zakrzewski, V. G.; Dapprich, S.; Daniels, A. D.; Strain, M. C.; Farkas, O.; Malick, D. K.; Rabuck, A. D.; Raghavachari, K.; Foresman, J. B.; Ortiz, J. V.; Cui, Q.; Baboul, A. G.; Clifford, S.; Cioslowski, J.; Stefanov, B. B.; Liu, G.; Liashenko, A.; Piskorz, P.; Komaromi, I.; Martin, R. L.; Fox, D. J.; Keith, T.; Al-Laham, M. A.; Peng, C. Y.; Nanayakkara, A.; Challacombe, M.; Gill, P. M. W.; Johnson, B.; Chen, W.; Wong, M. W.; Gonzalez, C.; Pople, J. A. *Gaussian 03, Revision C.02*; Gaussian, Inc., Wallingford, CT, 2004.
(33) Neese, F. et al. Orca 2.7.0. http://www.thch.uni-bonn.de/tc/orca/.
(34) (a) Parr, R. G.; Yang, W. *Density Functional Theory of Atoms and Molecules*; Oxford University Press: New York, 1989. (b) Ziegler, Z. *Chem. Rev.* **1991**, *91*, 651–667.
(35) (a) Becke, A. D. *J. Chem. Phys.* **1993**, *98*, 5648–5652. (b) Lee, C.; Yang, W.; Parr, R. G. *Phys. Rev. B* **1988**, *37*, 785–789.
(36) Andrae, D.; Häussermann, U.; Dolg, M.; Stoll, H.; Preuss, H. *Theor. Chim. Acta* **1990**, *77*, 123–141.
(37) Bauernschmitt, R.; Ahlrichs, R. *J. Chem. Phys.* **1996**, *22*, 9047–9052.
(38) González, C.; Schlegel, H. B. *J. Phys. Chem.* **1990**, *94*, 5523–5527.
(39) Faza, O. N.; Álvarez-Rodríguez, R.; Silva-López, C. *Theor. Chem. Acc.* **2011**, *128*, 647–661.
(40) Grimme, S. *J. Chem. Phys.* **2006**, *124*, 034108.
(41) Schaefer, A.; Horn, H.; Ahlrichs, R. *J. Chem. Phys.* **1992**, *97*, 2571–2577.
(42) Weigend, F.; Ahlrichs, R. *Phys. Chem. Chem. Phys.* **2005**, *7*, 3297–3305.
(43) Schwerdtfeger, P.; Dolg, M.; Schwarz, W. H. E.; Bowmaker, G. A.; Boyd, P. D. W. *J. Chem. Phys.* **1989**, *91*, 1762–1774.
(44) Weigend, F. *Phys. Chem. Chem. Phys.* **2006**, *8*, 1057–1065.
(45) Single-point PCM calculations have been performed on the optimized geometries at the B3LYP/6-31G(d)-SDD level, using CH_2Cl_2 as solvent. However, gas-phase energy values have been used in all our discussions, because of the large errors introduced in the calculation of solvation energies in charged systems. The calculated solvation energies (see Supporting Information) span, nevertheless, a limited range of 2.74 kcal/mol that would not alter any of the conclusions of the study.